Environ Earth Sci
DOI 10.1007/s12665-013-2406-z

SPECIAL ISSUE

Marble decay induced by thermal strains: simulations and experiments

Victoria Shushakova · Edwin R. Fuller Jr. · Florian Heidelbach · David Mainprice · Siegfried Siegesmund

Received: 3 February 2013 / Accepted: 7 March 2013
© Springer-Verlag Berlin Heidelberg 2013

Abstract Thermoelastic behavior of different marble types was analyzed using computational modeling and experimental measurements. Eight marble samples with different composition, grain size, grain boundary geometry, and texture were investigated. Calcitic and dolomitic marbles were considered. The average grain size varies from 75 μm to 1.75 mm; grain boundary geometry differs from nearly equigranular straight grain boundaries to inequigranular-interlobate grain boundaries. Four typical marble texture types were observed by EBSD measurements: weak texture; strong texture; girdle texture and high-temperature texture. These crystallographic orientations were used in conjunction with microstructure-based finite element analysis to compute the thermoelastic responses of marble upon heating. Microstructural response maps highlight regions and conditions in the marble fabric that are susceptible to degradation phenomena. This behavior was compared to the measured thermal expansion behavior, which shows increasing residual strains upon repetitive heating–cooling cycles. The thermal expansion behavior as a function of temperature changes can be classified into four categories: (a) isotropic thermal expansion with small or no residual strain; (b) anisotropic thermal expansion with small or no residual strain; (c) isotropic thermal expansion with a residual strain; and (d) anisotropic thermal expansion with residual strain. Thermal expansion coefficients were calculated for both simulated and experimental data and also modeled from the texture using the MTEX software. Fabric parameters control the amount and directional dependence of the thermal expansion. Marbles with strong texture show higher directional dependence of the thermal expansion coefficients and have smaller microstructural values of the maximum principal stress and strain energy density, the main precursors of microcracking throughout the marble fabric. In contrast, marbles with weak texture show isotropic thermal expansion behavior, have a higher propensity to microcracking, and exhibit higher values of maximum principal stress and strain energy density. Good agreement between the experimental and computational results is observed, demonstrating that microstructure-based finite-element simulations are an excellent tool for elucidating influences of rock fabric on thermoelastic behavior.

Keywords Marble · Calcite · Dolomite · Finite-element simulations · Thermal expansion anisotropy · EBSD · Maximum principal stress · Coefficients of thermal expansion

V. Shushakova (✉) · E. R. Fuller Jr. · S. Siegesmund
Geowissenschaftliches Zentrum der Universität Göttingen, Goldschmidtstrasse 3, 37077 Göttingen, Germany
e-mail: victoria.shushakova@gmail.com

F. Heidelbach
Bayerisches Geoinstitut, Universität Bayreuth, Universitaetsstrasse 30, 95447 Bayreuth, Germany

D. Mainprice
Géosciences Montpellier, UMR 5243-CC 60, Université Montpellier 2, Place E. Bataillon, 34095 Montpellier, France

Introduction

The wide use of marble began in Rome during the first century BCE. Its use continues today and is ubiquitous in façade claddings, interiors and exterior structures, and monuments. However, marble is affected by weathering and has limited durability. Numerous cases of marble

Published online: 28 March 2013

decay during environmental exposure have been investigated. For example, well-known buildings such as the Amoco building in Chicago (Trewitt and Tuchmann 1988), Finlandia Hall in Helsinki (Ritter 1992), the National Library in New York (Rabinowitzt and Carr 2012), and many others constructions made of marble shown progressive weathering. Weathering is typically expressed as bowing: fissuring of marble and hence, a loss of relief structure (Fig. 1). Therefore, the study of marble decay mechanisms is vital for protecting historical heritage (Fig. 2) and is also necessary from an economical perspective. Replacement of façade panels can be very expensive.

There is considerable discussion in the literature regarding the causes of marble degradation. Marble consists predominately of calcite and dolomite. Both minerals show a pronounced anisotropy in their coefficients of thermal expansion. Calcite expands in one direction along *c* axis upon heating, while contracting along the *a* axis, and upon cooling the dilation is in the opposite direction. Dolomite has positive values for the coefficients of thermal expansion, however, by different amounts, and thus expands or contracts in all directions upon heating or cooling, respectively. Therefore, dolomite should be more resistant to the deterioration in spite of its stiffer elastic behavior. Due to the large anisotropy in the coefficients of thermal expansion of both minerals, residual stresses develop between the adjacent grains upon changes of temperature, either an increase or a decrease. Even a small temperature changes can lead to the appearance of inelastic residual strain in thermally treated marble (Battaglia et al. 1993) and hence, to failure or degradation of the material. Kessler (1919) pointed out that upon repeated heating permanent change in the internal structure of the material is observed. Siegesmund et al.(1999, 2000, 2008); Zeisig et al.(2002); Ruedrich (2003); Koch and Siegesmund (2004); Luque et al. (2011) reported length changes of approximately 1 mm/m upon repeated heating and cooling cycles, and consequently to a loss of cohesion along the grain boundaries. Fig. 3 illustrates the opening of grain boundaries for two Carrara marbles deformed to a different degree. The Carrara marble (S7) is characterized by open grain boundaries and significant higher bowing (>11 mm/m) compared with the S1 (<1 mm/m). The samples belong to the university library (SUB) in Göttingen, Germany. The increase in the grain-boundary opening is further documented by the measured total porosity: 0.45 % for the S1 sample and 2.03 % for the S7 sample. Moreover, the pore size maximum moves towards larger pore radii with an increase in the amount of bowing (Siegesmund et al. 2008). The maximum pore diameter of the sample S7 is around 1 μm, and, therefore, in the range of capillary pores, while in sample S1 the maximum pores are significant smaller. The increase in porosity and the resulted bowing were caused by the thermal behavior of calcite crystals described above.

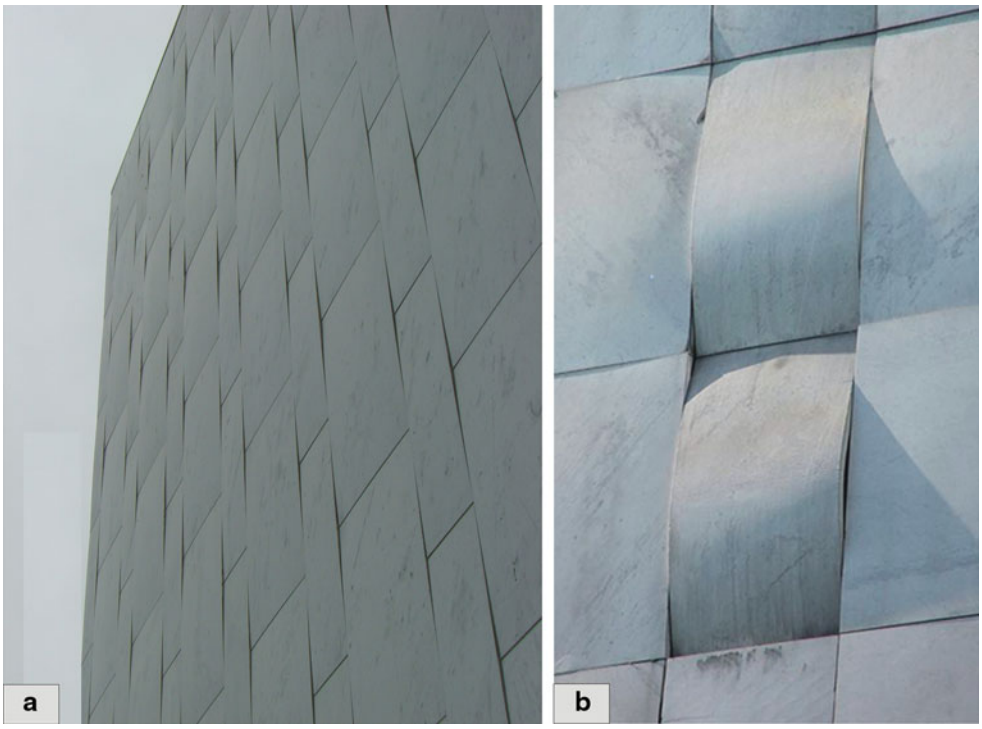

Fig. 1 **a** Deformed façade cladding made of Carrara marble from the Finlandia Hall in Helsinki and **b** details of a spectacular bowing phenomena of the Zagrepcanka building in Zagreb. Photo by bent Grelk and Jan Anders Brundin (www.geomasek.de und www.sp.se/building/team)

Fig. 2 **a** Marble Statuary from the Schlossbrücke, Unter den Linden (Berlin, Germany) "Nike instructs a boy in heroichistory" by Emil Wolff 1847 and **b** damage phenomena of intensive cracking and network of cracks (craquelling)

Microstructure-based finite-element simulations of the thermoelastic response of calcitic and dolomitic marbles to temperature changes (Weiss et al. 2002; Shushakova et al. 2012) have shown good agreement with experimental findings (Zeisig et al. 2002; Luque et al. 2011) and revealed that dolomite marbles have less propensity to degradation.

Influences of different fabric parameters on degradation were investigated by Widhalm et al. (1996); Tschegg et al. (1999); Siegesmund et al. (2000, 2008) ; Zeisig et al. (2002); Weiss et al. (2002, 2003, 2004); Saylor et al. (2007); Shushakova et al. (2011, 2012). These investigations showed that rock fabric greatly influences the thermal degradation of marble. Important fabric features include lattice-preferred orientation (LPO), shape preferred orientation (SPO), grain-boundary toughness, marble composition, grain size, grain-to-grain misorientation, and even directionality of the LPO with respect to the SPO.

For this investigation eight different well-known marbles with various fabric parameters were selected for a study of their thermoelastic behavior. Microstructure-based finite element simulations in combination with electron microscopy and experimental measurements of the thermal expansion behavior were used to elucidate the influence of rock fabrics on marble degradation. The finite-element simulations used the Object Oriented Finite element analysis of microstructures (OOF), developed at the National Institute of Standards and Technology (USA), to determine the thermoelastic responses of the marbles. Electron backscatter diffraction (EBSD) measurements were used to determine the microstructures and the crystallographic orientations of grains of the marble samples. Additionally, the directional dependence of the thermal expansion was computed with the MTEX software using the crystal texture measured by EBSD. The results are compared with the experimental data and numerical simulations. This approach is a test to predict the material behavior based on rock fabric data.

Methods and materials

Marble samples, microstructure and texture

To investigate the influence of rock fabric on marble decay eight various marble types were selected (Table 1). These marble types have been used as ornamental stones and exterior and interior cladding both in the past and in the present. They have different compositions, i.e. calcitic and dolomitic, vary in grain size from 75 μm to 1.75 mm and exhibit diverse texture types, notably weak texture, strong texture, girdle texture, and high-temperature texture.

A microstructure is required as an input for the finite element simulations. Microstructures and crystallographic orientations of grains were determined for the actual

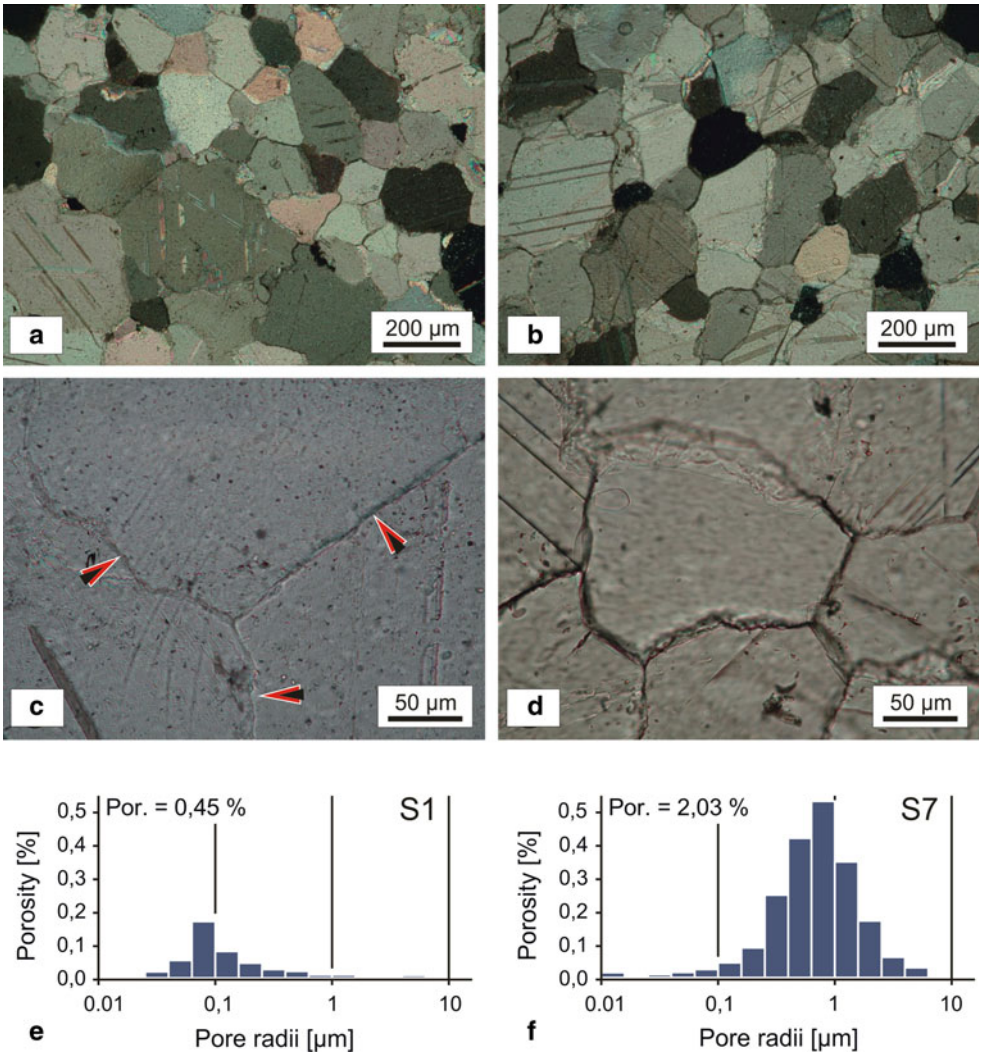

Fig. 3 Representative thin section images of **a** slightly deformed Carrara marble and **b** strongly deformed Carrara marble; **a**, **b** overview (crossed polarizers) and **c**, **d** details of the grain boundaries; **e** pore radii distribution of slightly deformed Carrara marble **f** pore radii distribution of strongly deformed Carrara marble. Shown in **e**, **f** is the percent of the porosity in each pore size range. The total porosity is shown in the insert

Table 1 Marble types, locations, and select fabric parameters

No.	Marble	Location	Composition	Average grain size
1	Thassos (Th)	Greece	Dolomitic	1.75 mm
2	Lasa (LA)	Italy	Calcitic	1 mm
3	Grechisches Volakas (G)	Greece	Calcitic	75–100 µm
4	Sölk (SK)	Austria	Calcitic	1.25 mm
5	Wachau (W)	Austria	Calcitic	1–1.5 mm
6	Arabescato Altissimo Carrara (AA)	Italy	Calcitic	200–300 µm
7	Bianco Carrara (BC)	Italy	Calcitic	150 µm
8	High-temperature Carrara (HT)	Italy	Calcitic	200–800 µm

marble samples using the electron backscatter diffraction (EBSD) technique. The procedure for measuring crystallographic orientations by EBSD and the manipulation of the EBSD data are described elsewhere (e.g., Halfpenny 2010). EBSD data for a marble section consist of an ordered data set of (*x, y*) coordinates and three Bunge Euler angles (Bunge 1985) for describing the rotation of the orientation of the crystalline material at each data point from the sample reference frame to the crystal reference frame. Single-crystal orientations were thereby measured on a grid with a step size of 20 µm, thus yielding an orientation map, or an Euler-angle map, where grain orientations are represented by a specific color (Fig. 4). In the present study the *XZ* plane was measured for all samples, where *X* is the direction of lineation and *Z* is the normal to the foliation planes.

To elucidate the influence of the texture on the thermoelastic response, pole figures for each marble sample were generated using the EBSD HLK Channel 5 software.

Four typical types of marble texture were observed: (a) weak texture (e.g., AA marble); (b) strong texture (e.g., SK marble); (c) girdle texture (e.g., LA marble); and high-temperature texture (e.g., HT marble). Examples of the {001} pole figure for select marble types are plotted in Fig. 5.

Leiss and Ullemeyer (1999) described fundamental calcite and dolomite texture types as *c* axis and *a* axis fiber type, or overlapping combinations of these two texture types. Later Leiss and Molli (2003) found one more type of texture, called high-temperature texture in natural marbles of Carrara. Carrara marbles AA and BC show weak *c* axis fiber texture with a maximum of the multiples of random distribution (MRD) of 1.39 and 1.33, respectively. Sölk marble exhibits *c* axis fiber type and shows a strong *c* axis maximum of 3.32 MRD. Two other types of texture were observed by the EBSD measurements. The *c* axis of Lasa marble shows a girdle distribution (*a* axis fiber type), while a naturally deformed Carrara marble (HT) exhibits a high-temperature texture, which is characterized by double maximum of the *c* axis with a bisecting line normal to the share plane (for details see Leiss and Molli 2003). Grechisches Volakas marble and Thassos marble exhibit *c* axis fiber texture with a *c* axis maximum of MRD of 3.63 to MRD of 7.6, respectively. The texture type of Wachau marble was found by Zeisig et al. (2002) and determined as a *c* axis fiber texture with tensor shape $T = -0.859$ ($T = -1$ corresponds to a perfectly linear *c* axis distribution).

Image processing

As EBSD maps are collected automatically, the data often contain non-indexed points, i.e., data points for which the crystallographic orientation could not be determined. Four methods were developed to handle these non-indexed data points. The simplest method is to give these data points the crystallographic orientation of the sample reference frame. This approximation is not correct, but when the number of undefined points is sparse, the results are not significantly different from a correct value. Nonetheless, this method was not generally used. A better approximation is to treat these undefined data points as voids. Indeed, some of the undefined data points are most likely voids. This approximation works well for most finite element meshes, but empty finite elements (i.e., elements with elastic constants which are zero) can lead to numerical instabilities in the finite element solver. To avoid these numerical instabilities, a third approximation was to assign soft isotropic elastic properties to these void regions. Typically, a Young's modulus of 0.001 GPa and a Poisson's ratio of zero were used to model these soft (stabilizing) void space elements. To verify that this approximation has minimal influence on the results, meshes that were solvable when empty elements were used were also tested using soft isotropic elements for the voids. The thermoelastic responses computed for both cases were in excellent agreement; the differences were typically less than 0.1 %. Here, when the number of undefined data points was small, simulations were typically performed using these soft isotropic elements to model the void space.

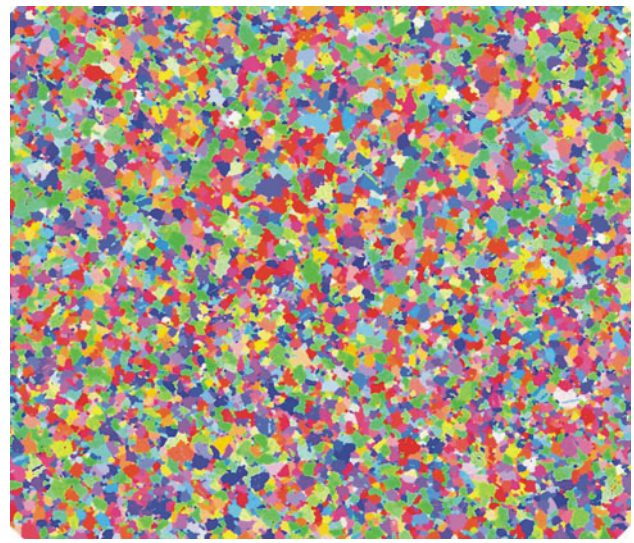

Fig. 4 Microstructure of Arabescato Altissimo Carrara (*AA*) marble used for the finite-element simulations. The average grain size is 200 to 300 μm. The color mapping indicates the grain orientation

In several cases (e.g., the Thassos marble sample) the undefined regions are clearly not voids, but are regions where the sample for some reason (e.g., large deformation or missing pieces) did not index properly. For these samples a fourth method was developed to clean the EBSD images. A Voronoi decomposition algorithm was developed whereby defined data regions adjacent to an undefined region randomly expand into the undefined nearest-neighbor region. This process continues until all of the undefined regions are consumed by the surrounding defined regions. The result is a cleaned EBSD microstructure with no undefined regions. A computer program written in Perl was used to implement this algorithm. A comparison of an original EBSD Euler map (the black areas are the undefined regions) and a cleaned version of this image is presented in Fig. 6 for a Thassos marble. This procedure of cleaning the microstructure is used for all EBSD data sets which have a relatively large number of undefined data points.

Finite-element simulations

The object-oriented finite-element method (OOF) developed at the National Institute of Standards and Technology (USA) (Carter et al. 1998; Langer et al. 2001) was used for the finite-element simulations. The OOF software is in the public domain. Source code and manuals are available at:

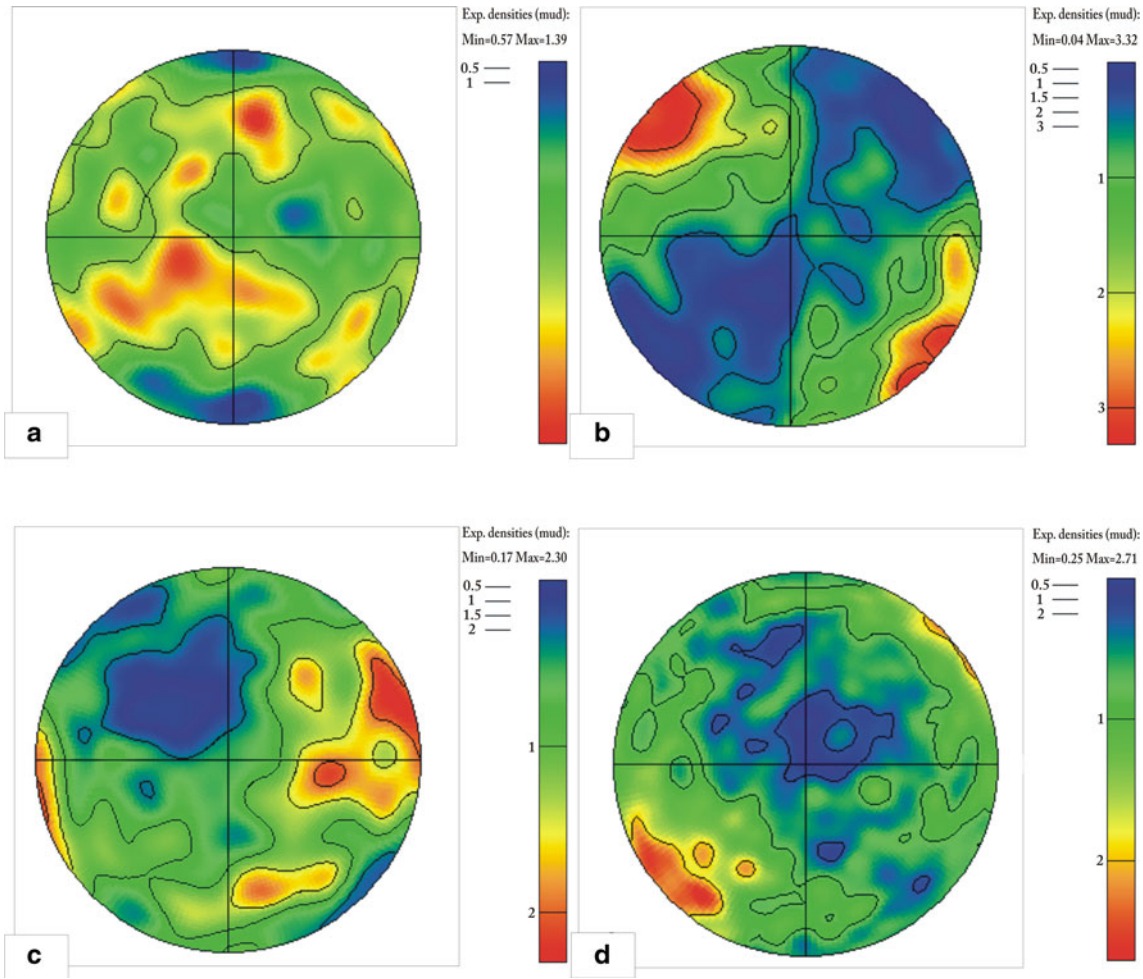

Fig. 5 {001} Pole figures from the EBSD HLK Channel 5 software for marble samples in *XZ* planes: **a** Arabescaro Altissimo Carrara marble (weak texture); **b** Sölk marble (strong texture); **c** Lasa marble (girdle texture); **d** High-Temperature Carrara marble (high-temperature texture)

http://www.nist.gov/mml/ctcms/oof/. The OOF1 software was used here.

A simple meshing algorithm was applied to create a finite-element mesh. Each EBSD data point, or image pixel on the EBSD orientation map, was converted into two triangular elements. The diagonal dividing each pixel was alternated from pixel to pixel so that the orientations of the right-triangle elements were not all the same. More details of finite-element meshing procedure in OOF can be found in Langer et al. (2001), Weiss et al. (2002), Chawla et al. (2003), Saylor et al. (2007), Wanner et al. (2010).

Typical EBSD data files for measured marbles contain 700 × 600 pixels, or 420,000 (x, y) coordinates (or pixels) with a step size 20 μm. A simple mesh would have 840,000 elements. As computer resources were not available to solve this mesh, the images were cropped into nine subsections of 200 × 200 pixels by cropping 50 pixels off either side of the 700 pixel width. An example is shown in Fig. 7 for a Lasa calcitic marble sample.

The subsections of the EBSD data sets were converted into the pixel-based triangular finite element mesh with the thermoelastic properties of the constituent marble. The result is a triangular finite-element mesh with each element having the thermoelastic properties (i.e., the fourth-rank elastic constant tensor and second-rank thermal expansion tensor) of either dolomite or calcite marble with the crystallographic thermoelastic tensors rotated to the sample reference frame by the Euler rotations for that pixel data point. The single crystal elastic constant tensors for both minerals, $\boldsymbol{C}_{ij}$, (Bass 1995) and the crystalline coefficients of thermal expansion for calcite (Kleber 1959) and dolomite (Reeder and Markgraf 1986) are given in Table 2.

The crystallographic orientations obtained by EBSD are given via three Euler angles. To convert the Bunge definition of Euler angles in the Euler angle definition used in OOF1, the following equations were used:

$$\alpha = \Theta$$

$$\beta = \text{mod}\ [90 - \varphi_2,\ 360]$$

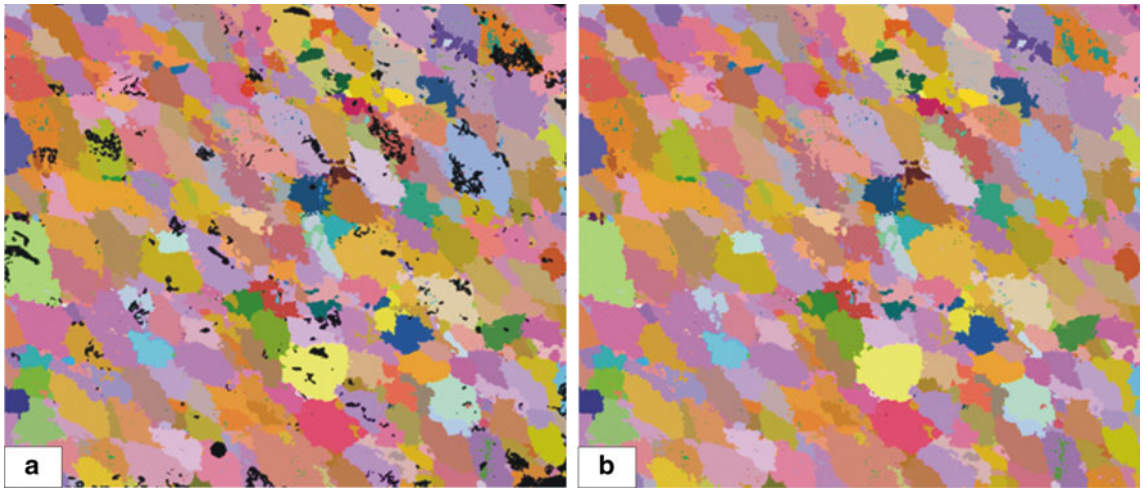

Fig. 6 Two images of a Thassos marble sample: **a** original EBSD Euler-angle map (the *black regions* are the *undefined* regions); and **b** a *cleaned* EBSD Euler-angle map

γ=mod [90−φ_1, 360]

where (α, β, γ) are the input Euler angles in OOF1 and (φ_1, Θ, φ_2) are Bunge angles, and the mod function is a function that returns the remainder of a number n after it is divided by a divisor d:mod [n, d] = $n-d \times$ int [n/d]where the *int* function is a function that rounds a number down to the closest integer.

With the undefined regions cleaned by one of the methods given above, thermoelastic responses were computed for each of the subsections of the EBSD data sets for the misfit strains produced by a 100 °C temperature change. The finite-element calculations are based on two-dimensional elasticity with a plane-stress assumption, and thereby simulated the results for a free surface. The typical thermoelastic responses that are computed are the maximum principal stress and the elastic strain energy density. Thermal expansion coefficients were calculated as well from the dilations of the subsection in both the X and Z directions.

Thermal expansion measurements

To replicate temperature changes observed in nature on building stones, thermal expansion measurements were performed in the temperature range of 20 °C to 90 °C using a pushrod dilatometer (for details see Koch and Siegesmund 2004). The three main components of the dilatometer are (1) the specimen holder in a climate chamber, (2) the heating unit, and (3) the displacement register. The displacement sensors are able to determine length changes of ±1 µm. Thus, a final residual strain of about 0.02 mm/m could be resolved for sample with a length of 50 mm. A quartz glass sample was used to calibrate the dilatometer.

The samples were heated from 20 to 90 °C and then cooled to the initial temperature of 20 °C; each cycle lasting 14 h and 20 min. Four repeating heating–cooling cycles were performed (Fig. 8). The experimental setup allows the thermal dilatation of up to six samples to be measured simultaneously at same conditions. In the present study the six specimens were cut in the *X, Y, Z, XY, XZ,* and *YZ* directions for each marble type. The dilatometry samples were cylinders 15 mm in diameter and 50 mm in length.

The experimental coefficient of thermal expansion coefficient (α_{expt}) is determined from the first heating cycle by the following equation:

$$\alpha_{expt} = \frac{\Delta\ell_0}{\ell_0 \times \Delta T}$$

where $\Delta\ell_0 = [\ell(90\,°C) - \ell(20\,°C)]$ is the sample length change during the first heating cycle, $\ell_0 = \ell(20\,°C)$ is the original sample length, and $\Delta T = 90 - 20\,°C$ is the temperature differential. The usual units of the coefficients of thermal expansion here are 10^{-6} K^{-1}. The residual strain (ε_r in mm/m) is determined as the ratio between the sample length change $\Delta\ell_r$ after the four complete heating–cooling cycles and the initial length of the sample ℓ_0:

$$\varepsilon_r = \frac{\Delta\ell_r}{\ell_0}$$

Calculation of polycrystalline thermal expansion properties

To calculate the thermal expansion properties of a polycrystalline aggregate of calcite or dolomite one needs the single crystal tensor (α_{ij}), LPO data, and some knowledge of the individual grain areas in two dimensions. LPO data

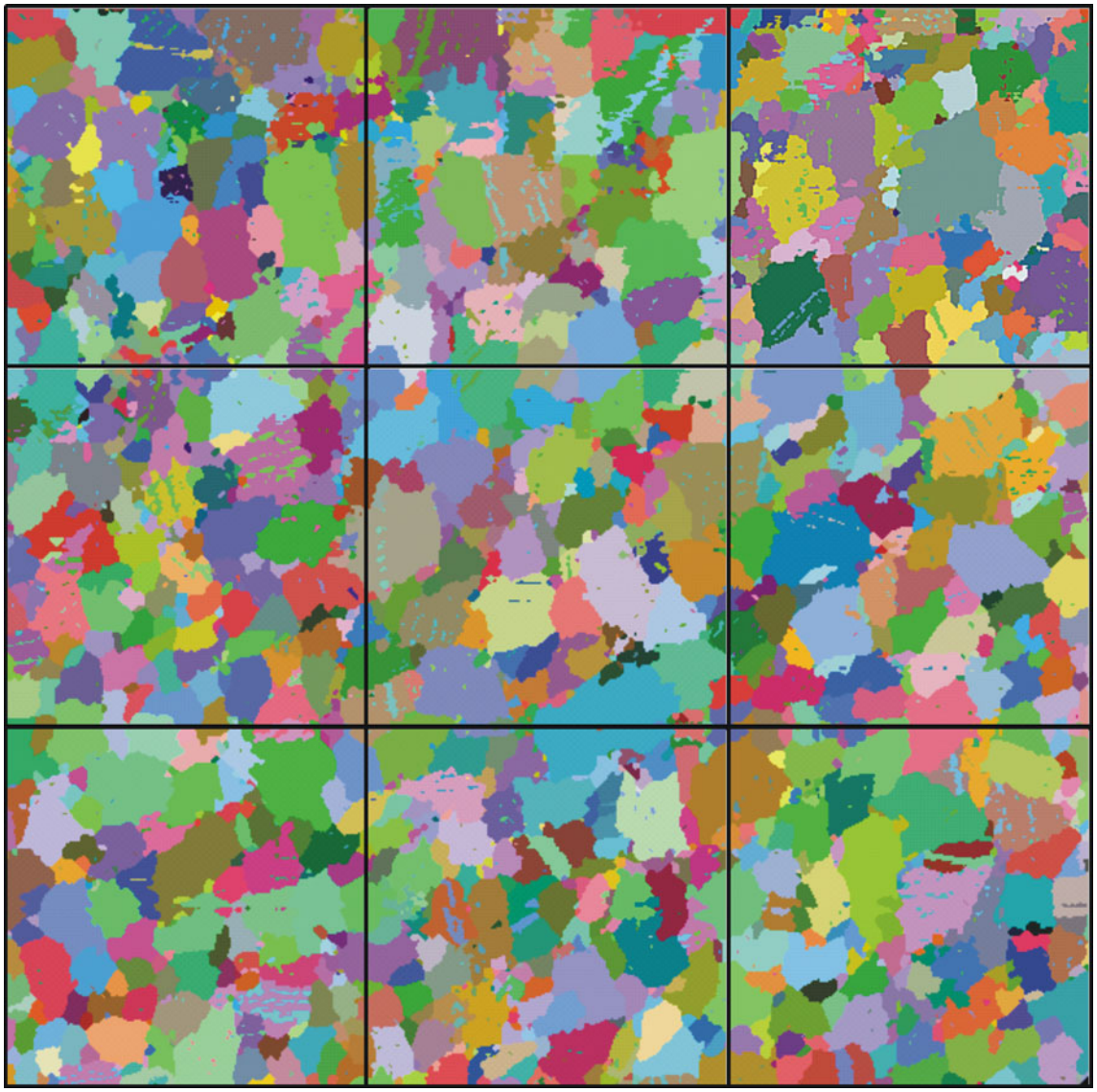

Fig. 7 EBSD Euler-angle microstructural map for the Lasa calcitic marble, which has been subdivided into nine 200 × 200 pixel subsections. The color mapping shows the crystal orientation of each data point via the Bunge Euler angles (φ_1, Θ, φ_2) which are mapped into the (*red, green, blue*) color of each pixel by the mapping given: red = 256 $\varphi_{1/180}$; green = 256 $\Theta/180$; blue = 256 $\varphi_{2/120}$

Table 2 Elastic constants for calcite and dolomite, $\boldsymbol{C_{ij}}$, in GPa (Bass 1995) and the crystalline coefficients of thermal expansion, $\boldsymbol{\alpha_{ij}}$, in 10^{-6} K^{-1} for calcite (Kleber 1959) and dolomite (Reeder and Markgraf 1986)

Material	C_{11}	C_{12}	C_{13}	C_{14}	C_{15}	C_{33}	C_{44}	α_{11}	α_{33}
Calcite	144.0	53.9	51.1	−20.5	0	84.0	33.5	−6.0	26.0
Dolomite	205	70	57.4	−19.5	13.7	113.0	39.8	6.0	26.0

measured in the form of EBSD orientation maps are very suitable for estimating anisotropic physical properties as the orientation data are weighted by the fractional surface area. A map pixel with an orientation ($\mathbf{g}$) and surface area (δA) is the smallest map component. The first step in the calculation of thermal expansion properties of a polycrystalline aggregate is the rotation of the single crystal tensor α_{ij} into the orientation of the map pixel by the inverse rotation matrix $\mathbf{g}^{-1} = \mathbf{g}^{\text{Transpose}}$

$$\alpha_{ij}(\mathbf{g}) = \mathbf{g}_{ki} \times \mathbf{g}_{lj} \times \alpha_{kl}$$

where $\alpha_{ij}(\mathbf{g})$ is thermal expansion tensor in the sample, or pole figure coordinates and $\mathbf{g} = \mathbf{g}(\varphi_1, \Theta, \varphi_2)$ is the rotation matrix from the sample coordinate system to the crystal

coordinate system defined by the Bunge Euler angles φ_1, Θ, and φ_2. The second step is to sum the contribution of all the tensors associated with each map pixel,

$$\alpha_{ij} = \sum (\delta A/A) \times \alpha_{ij}(\mathbf{g})$$

where α_{ij} is the ensemble average of the thermal expansion tensors of the pixels and $(\delta A/A)$ is the fractional area of each pixel. This average corresponds to the Voigt average of elasticity. The thermal expansion of the polycrystalline sample in any pole figure direction X is given by

$$\alpha(X) = \alpha_{ij} \times X_i \times X_j$$

In the present case, experimental measurements were made of thermal expansion of the samples in various directions. To compare these measurements with the ensemble average thermal expansion calculated from the EBSD data, the reference frame of the experimental thermal expansion tensor needs to be rotated into coincidence with the frame of EBSD calculated tensor. Normally this would be complex task, but in the case of a 2nd rank symmetrical tensor, like the thermal expansion tensor, it has an intrinsic orthogonal reference frame given by the 3 eigenvectors of the tensor. The eigenvectors correspond to the directions with the maximum, intermediate, and minimum eigenvalues of the tensor. The angles between the eigenvectors of the experimental tensor and the EBSD tensor allow the construction of a transformation matrix R and the application of the formula,

$$\alpha_{ij}^{\mathrm{EBSD}} = R \times \alpha_{ij}^{\mathrm{Expt}} \times R^{\mathrm{Transpose}}$$

to calculate the experimental tensor in the same frame as the EBSD tensor. All of these calculations were done using MTEX, the open-source MATLAB toolbox for texture analysis (Hielscher and Schaeben 2008), which has been extended for the calculation of 2nd and 4th rank tensors of anisotropic physical properties (Mainprice et al. 2011).

Results and discussion

Microfabric

The microfabric analysis is based on microstructures which were obtained by EBSD measurements. The microfabric will be discussed for Carrara marbles AA and BC, Sölk marble, Lasa marble, and HT Carrara marble, because they exhibit diverse thermal expansion behavior and serve the examples of four different types of thermal expansion behavior. The Arabescato Altissimo (AA) and Bianco Carrara (BC) marbles are fine-grained marbles that show nearly equigranular straight grain boundaries (i.e., a foam structure) with an average grain size of 150–300 µm, whereas Lasa (LA) and Sölk (SK) marbles are coarse grained, with average grain sizes of 1 mm and 1.25 mm, respectively, and exhibit inequigranular-interlobate grain boundaries. High-Temperature Carrara (HT) marble shows inequigranular-polygonal grain boundaries, and the grain size varies from 200 to 800 µm. The microfabrics are presented in Fig. 9. For more detailed microfabric analysis, see Zeisig et al. (2002), Leiss and Molli (2003), Siegesmund et al. (2008).

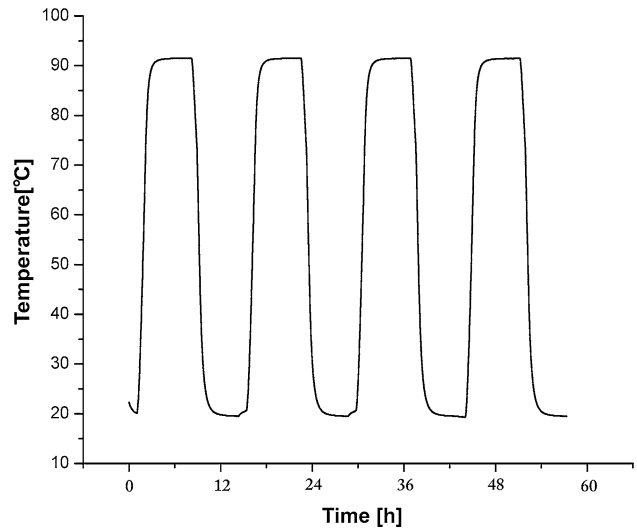

Fig. 8 Temperature as a function of time. Four heating–cooling cycles were performed at a rate of 1 °C/min

Thermal dilatation and residual strains

Thermal dilatation (in mm/m) describes the relative change of the sample's length (Grüneisen 1926). The investigated marble samples showed different types of thermal dilation behavior and residual strain behavior. Previous studies (Siegesmund et al. 2000; Zeisig et al. 2002; Ruedrich 2003) have shown that distinct marble groups can be distinguished according to their thermal dilation and residual strain behavior under thermal treatment. The four types (after Siegesmund et al. 2008) are used to classify the marbles investigated here. These types are shown in Table 3 along with the representative marbles investigated here.

Figure 10 illustrates the thermal expansion and residual strain behavior for marble samples Arabescato Altissimo Carrara marble (AA), Sölk marble (SK), Bianco Carrara marble (BC), and High-Temperature Carrara marble (HT), and their dependence on the *X, Y, Z* directions upon four repeated heating–cooling cycles. Carrara marbles AA and BC exhibit isotropic thermal expansion, as there is a less pronounced directional dependence of the thermal expansion, for example in comparison with the SK, which has strong directional dependence. For the Arabescato

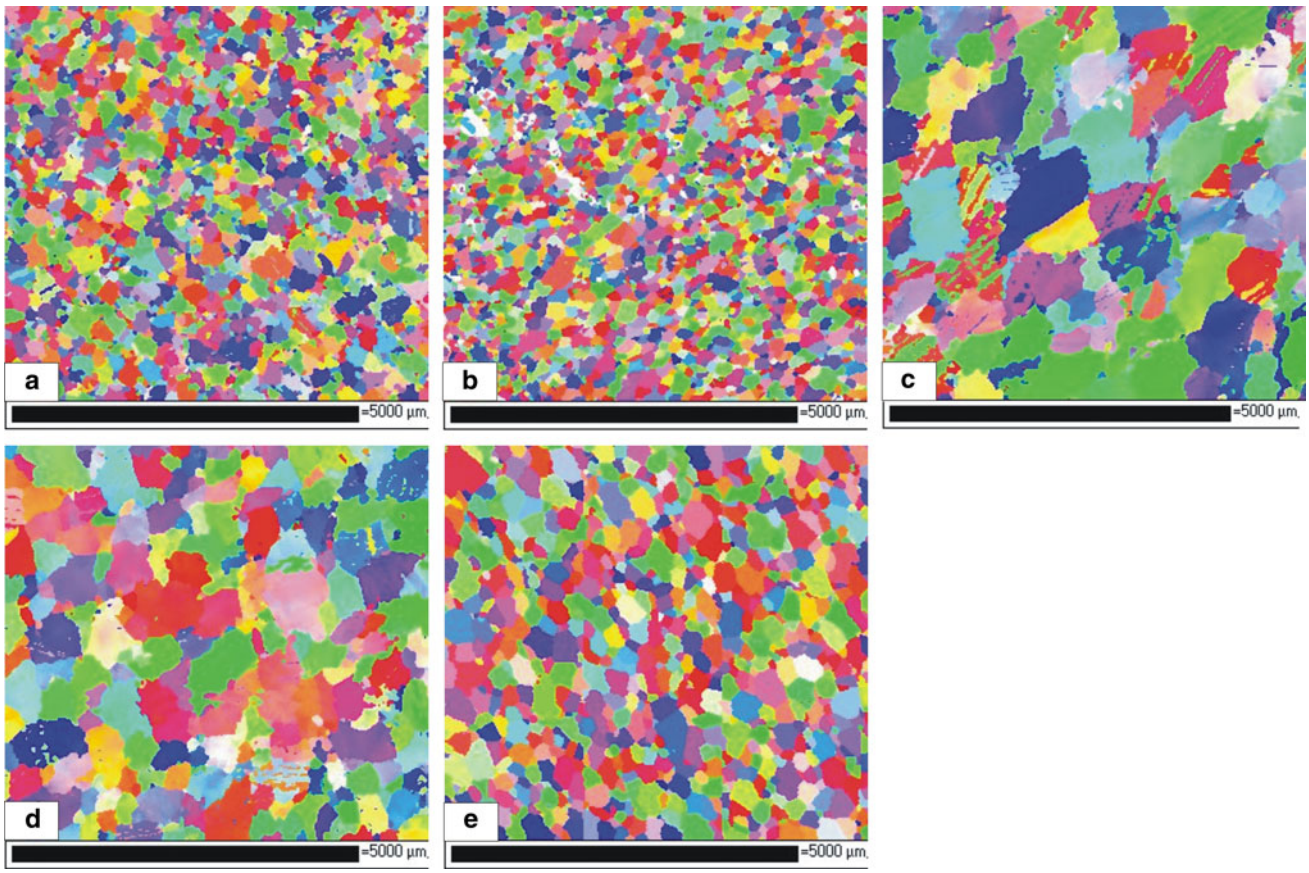

Fig. 9 Marble microfabric: **a** Arabescaro Altissimo marble (*AA*); **b** Bianco Carrara marble (*BC*); **c** Sölk marble (*SK*); **d** Lasa marble (*LA*); **e** high-temperature Carrara marble (*HT*). The microfabric is shown as a cropped selection (305 × 285 pixels) from microstructures obtained by EBSD in XZ plane of marble samples

Table 3 Marble classification according to thermal expansion and residual strain behavior after Siegesmund et al. (2008)

	Isotropic thermal expansion	Anisotropic thermal expansion
Without residual strain	Type (a)	Type (b)
	Arabescato Altissimo	Sölk (SK)
	Carrara (AA)	Thassos (Th)
		Wachau (W)
With residual strain	Type (c)	Type (d)
	Bianco Carrara (BC)	Lasa (LA)
		Grechisches Walakos (G)
		High-temperature Carrara (HT)

Altissimo Carrara marble the maximum residual strain after four cycles is −0.03 mm/m, while for the Bianco Carrara marble a larger expansion of 0.1 mm/m is observed. The behavior of the Lasa marble is different. The smallest thermal expansion (0.06 mm/m) is observed for the *Y* direction and the largest expansion (0.12 mm/m) is observed for *Z* direction. High-temperature Carrara marble exhibits the largest residual strain of all the investigated marbles. The *Z* direction sample has a residual strain of 0.4 mm/m (0.04 %). The Sölk marble (SK) sample shows anisotropic behavior with small residual strain. The maximum residual strain for the SK sample after four cycles is 0.03 mm/m (0.003 %) and is in the *X* direction.

The influence of crystalline texture is evidenced in the thermal dilatation behavior of marbles (Ruedrich et al. 2002; Zeisig et al. 2002; Siegesmund et al. 2008). The Carrara marbles, which exhibit isotropic thermal expansion behavior, have the smallest maxima of multiples of random distribution (MRD) in their pole figures with maximum MRD = 1.39 for AA and maximum MRD = 1.33 for BC. In contrast, Sölk marble (SK) with a *c* axis maximum MRD of 3.32 has a strong directional dependence on its thermal

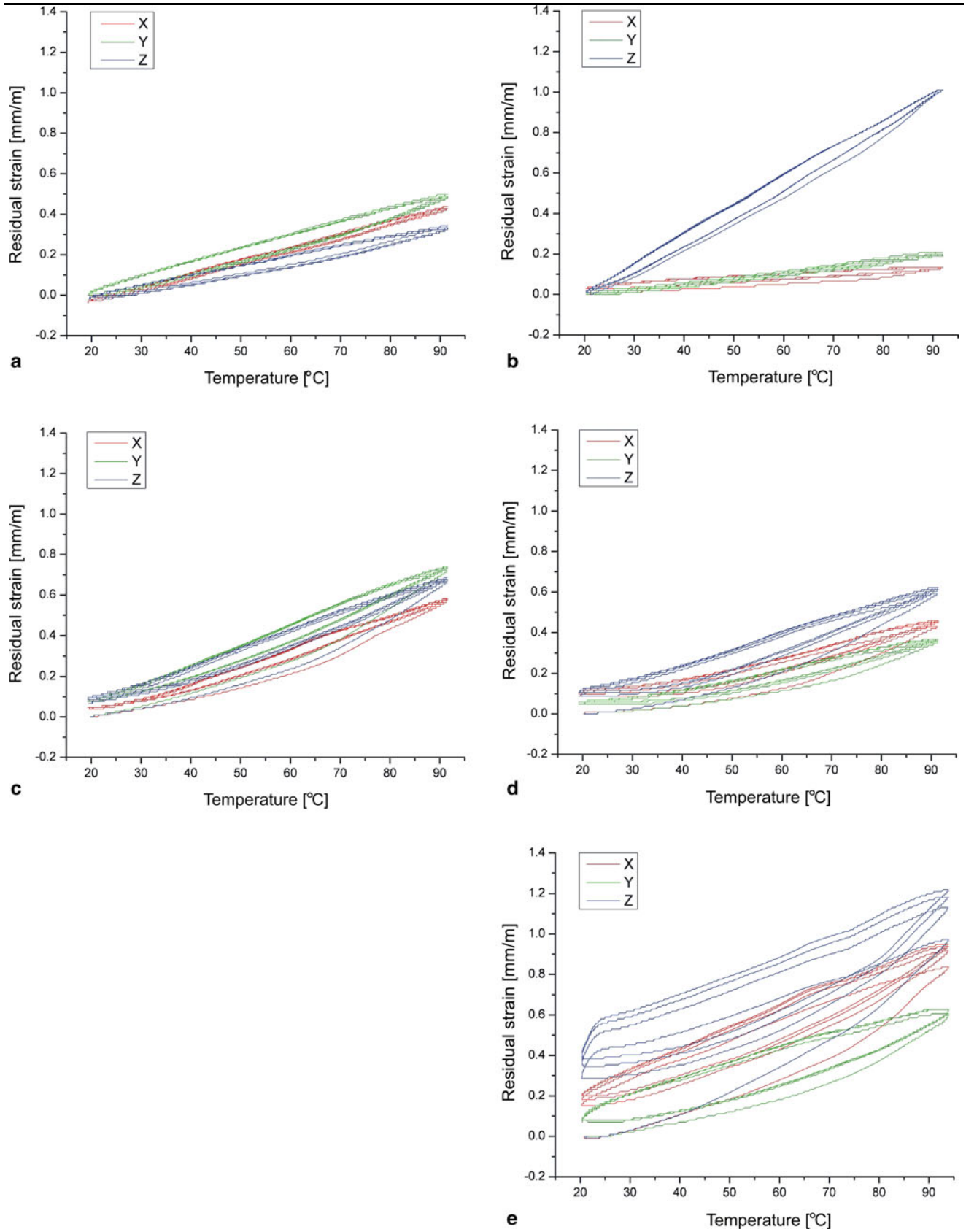

Fig. 10 Experimentally determined residual strain as a function of temperature: **a** Arabescaro Altissimo Carrara marble (*AA*); **b** Sölk marble (*SK*); **c** Bianco Carrara marble (*BC*); **d** Lasa marble (*LA*); **e** high-temperature Carrara marble (*HT*). The curves are given for *X*, *Y*, and *Z* directions

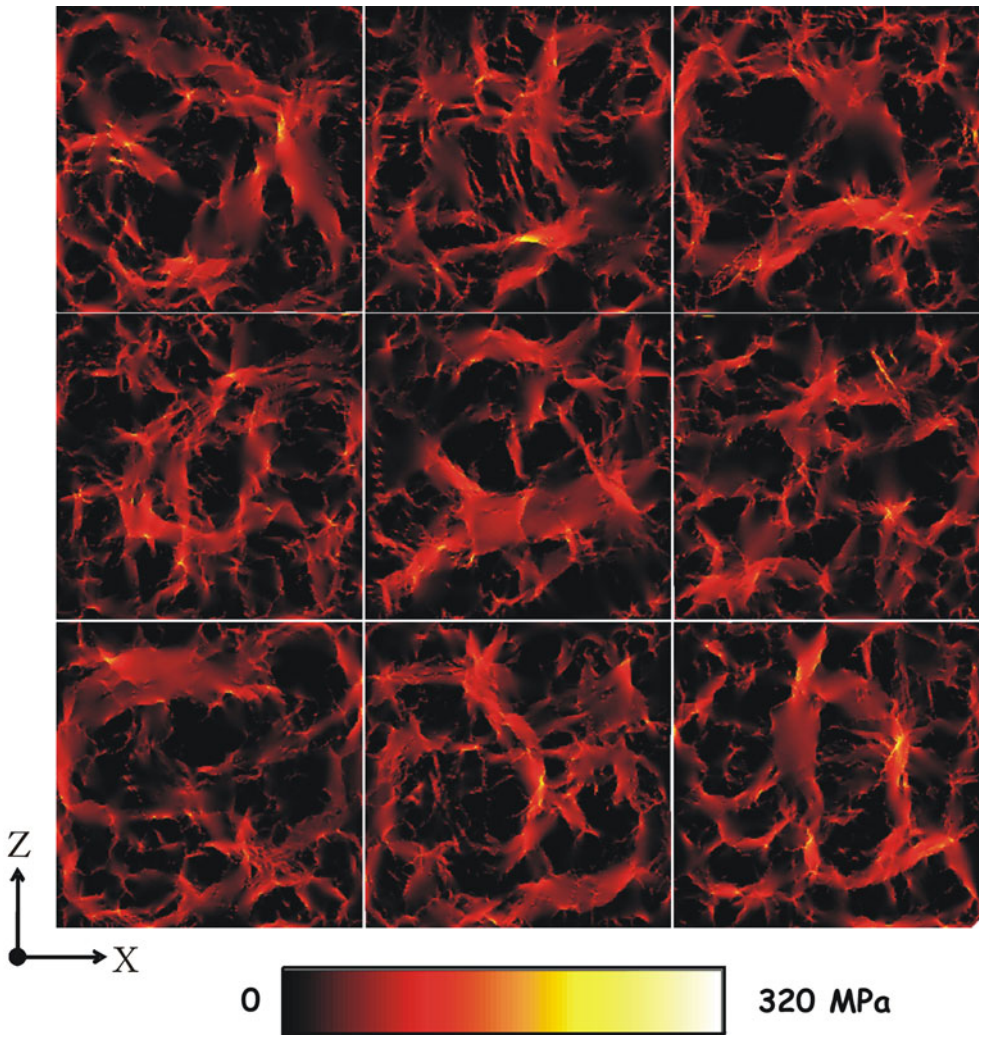

Fig. 11 Thermoelastic response maps showing the spatial dependence of the maximum principal stress for each of the nine subsections of the EBSD Euler-angle map for the Lasa calcitic marble shown in Fig. 7. The reference frame used for the finite-element simulations is given

expansion behavior. The impact of grain size is not significant in the present study. The coarse-grained marble such as SK shows almost no residual strain, while both fine-grained Carrara marbles AA and BC exhibit difference in thermal expansion behavior, notably for AA the residual stress is almost zero and BC has expansion of 0.1 mm/m. The medium-grained size HT Carrara marble has the largest thermal dilatation, which expands to 0.4 mm/m. The role of grain boundaries is also not important (Zeisig et al. 2002; Siegesmund et al. 2008). The HT Carrara marble with polygonal structure as well as the Lasa marble with interlobate grain boundaries both have a residual strain.

Thermoelastic response

Thermoelastic response maps for each of the marbles were generated for the nine subsections of the EBSD maps. Maximum principal stress maps for the nine subsections in Fig. 7 are shown in Fig. 11. From each response map the average thermoelastic response for that subsection and its standard deviation over that subsection (the microstructural standard deviation) were computed. The average value of the nine subsection values and its standard deviation were computed. Additionally, the coefficients of thermal expansion for each subsection were computed for both the *X* and *Z* directions and averaged over the nine subsections. These values will be compared with the experimentally measured values for these marbles samples.

The results indicate that the smallest maximum principal stress 18.7 ± 2.5 MPa is observed for the Thassos dolomitic marble. The difference between dolomitic and calcitic marbles can be explained by the thermal expansion anisotropy and the differences in the single-crystal elastic constants of these two major rock-forming minerals. While dolomite is stiffer than calcite, calcite has a greater thermal expansion anisotropy resulting in a higher maximum principal stress.

The largest values of the average maximum principal stress (35.0 ± 0.5 and 34.9 ± 0.9 MPa) were observed for the Arabescato Altissimo (AA) and Bianco Carrara (BC) marble, respectively, where only a weak preferred orientation is evident (maximum MRD = 1.39 for AA and

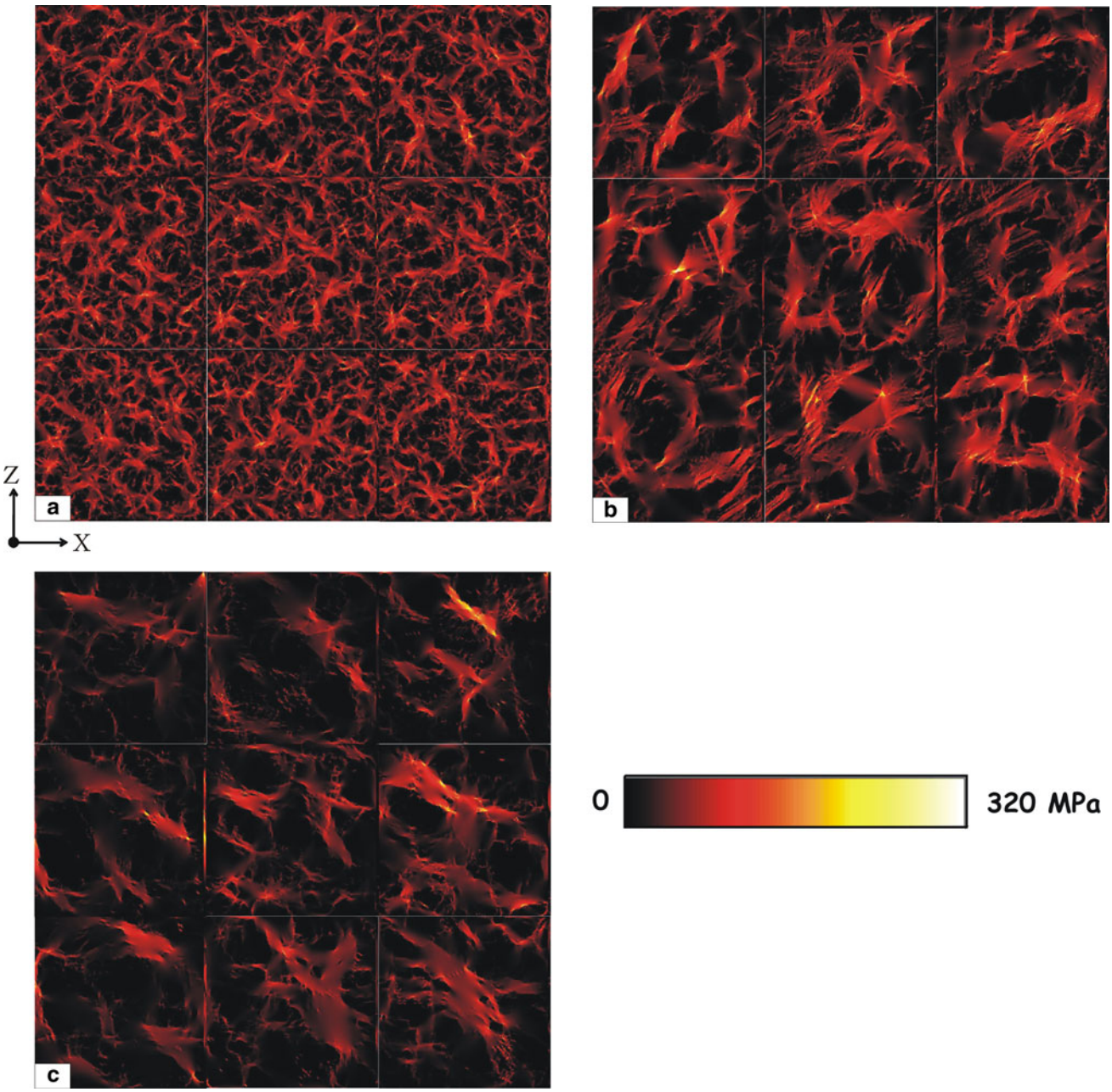

Fig. 12 Thermoelastic response maps showing the spatial dependence of the maximum principal stress for each of the stiched together nine subsections of the EBSD Euler-angle map for **a** AA calcitic marble with weak texture (MRD = 1.39); **b** SK calcitic marble with strong texture (MRD = 3.32); **c** Th dolomitic marble with strong texture (MRD = 7.6)

maximum MRD = 1.33 for BC). The High-Temperature Carrara marble shows a comparable value of the average maximum principal stress (34.6 ± 1.5 MPa), while the Sölk marble, which has a much more pronounced LPO with a maximum MRD of 3.32, exhibits a smaller value of average maximum principal stress (29.9 ± 1.2 MPa). Lasa marble with girdle texture (and maximum MRD of 2.3) shows an average maximum principal stress of 31.0 ± 1.0 MPa. Figure 12 illustrates the difference between maximum principal stress maps for marbles with weak and strong texture and the influence of marble composition as well. In Shushakova et al. (2012) it was revealed that regions with high maximum principal stress in the uncracked state correspond to microcracks in the cracked material. The Thassos marble shows fewer regions with high maximum principal stress in comparison to the AA and SK marbles (Fig. 12), i.e. its propensity of microcracking is less. In agreement with the results for the idealized microstructures (Shushakova et al. 2011), increasing LPO leads to a decrease in the observed maximum

Table 4 Thermal expansion coefficients for investigated marbles: averaged from the nine subsections computed from the finite-element simulations α_{OOF} with standard deviation, calculated from thermal expansion measurements α_{expt}, in the sample reference frame and in the EBSD reference frame, and modeled from textures applying Voigt model α_{Voigt}

Marbles	α_{OOF}, $10^{-6}K^{-1}$	α_{expt}, $10^{-6}K^{-1}$		α_{Voigt}, $10^{-6}K^{-1}$
		in the sample reference frame	in the EBSD reference frame	
AA	$\alpha_x = 4.4 \pm 0.5$ $\alpha_z = 3.5 \pm 0.6$	$\alpha_x = 6.3$ $\alpha_z = 5.0$	$\alpha_x = 6.9$ $\alpha_z = 4.8$	$\alpha_x = 4.9$ $\alpha_z = 4.1$
BC	$\alpha_x = 3.7 \pm 0.4$ $\alpha_z = 3.7 \pm 0.4$	$\alpha_x = 8.0$ $\alpha_z = 9.2$	$\alpha_x = 8.6$ $\alpha_z = 8.8$	$\alpha_x = 4.3$ $\alpha_z = 4.3$
LA	$\alpha_x = 6.7 \pm 1.6$ $\alpha_z = 2.6 \pm 0.8$	$\alpha_x = 6.0$ $\alpha_z = 8.3$	$\alpha_x = 8.0$ $\alpha_z = 6.0$	$\alpha_x = 7.1$ $\alpha_z = 3.5$
HT	$\alpha_x = 5.7 \pm 0.7$ $\alpha_z = 4.5 \pm 0.8$	$\alpha_x = 11.6$ $\alpha_z = 13.5$	$\alpha_x = 13.0$ $\alpha_z = 12.0$	$\alpha_x = 6.3$ $\alpha_z = 5.2$
SK	$\alpha_x = 6.4 \pm 2.3$ $\alpha_z = 4.5 \pm 1.1$	$\alpha_x = 1.9$ $\alpha_z = 14.4$	$\alpha_x = 8.5$ $\alpha_z = 6.3$	$\alpha_x = 6.8$ $\alpha_z = 5.0$
Th	$\alpha_x = 12.9 \pm 0.7$ $\alpha_z = 15.6 \pm 0.9$	$\alpha_x = 14.0$ $\alpha_z = 4.7$	$\alpha_x = 8.0$ $\alpha_z = 9.7$	$\alpha_x = 12.9$ $\alpha_z = 15.1$
W	$\alpha_x = 4.2 \pm 1.1$ $\alpha_z = 5.7 \pm 0.9$	$\alpha_x = 6.2$ $\alpha_z = 9.7$	$\alpha_x = 5.8$ $\alpha_z = 8.0$	$\alpha_x = 3.3$ $\alpha_z = 5.3$
G	$\alpha_x = 9.4 \pm 0.6$ $\alpha_z = 0.8 \pm 0.7$	$\alpha_x = 11.2$ $\alpha_z = 13.4$	$\alpha_x = 13.6$ $\alpha_z = 10.4$	$\alpha_x = 9.3$ $\alpha_z = 0.8$

Values are given in units of 10^{-6} K^{-1}

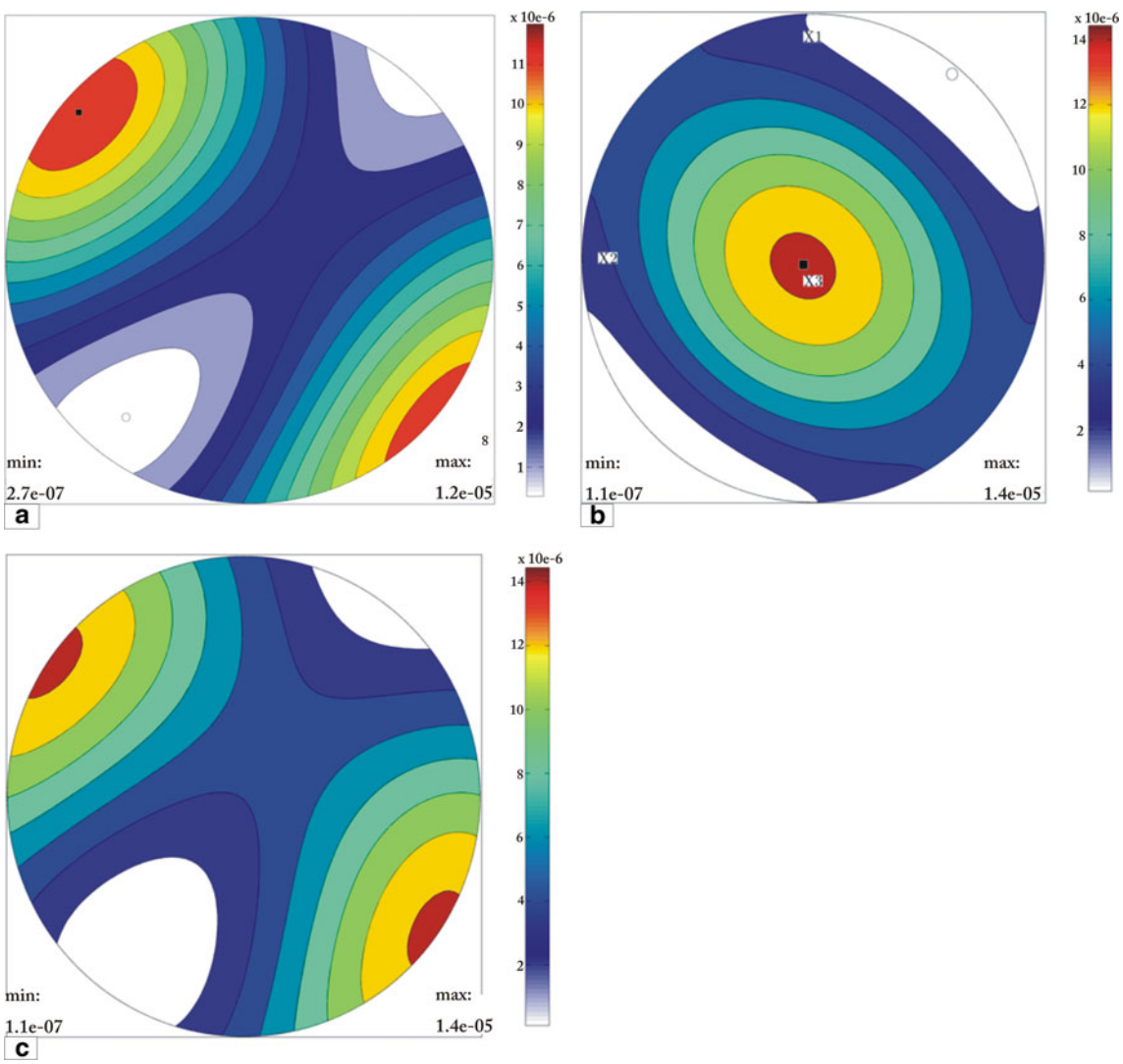

Fig. 13 Pole figure projection of the thermal expansion tensor for SK marble: **a** the plot of the thermal expansion Voigt average tensor derived from the texture in the frame of the EBSD data **b** the plot of the experimental thermal expansion tensor in the sample reference frame, **c** the plot of the rotated experimental thermal expansion tensor to the EBSD frame

principal stress and dolomitic marbles show smaller maximum principle stress and hence are more resistant against thermal degradation (Shushakova et al. 2011, 2012).

Thermal expansion: correlation between modeled and experimental results

In OOF simulations the coefficients of thermal expansion were calculated for each of the marbles. They were computed for the nine subsections of the EBSD maps and then averaged. The thermal expansion coefficient in the *X* direction, α_{x_OOF}, is calculated as the relative displacement change of the right and left sides of each of nine subsections. The thermal expansion coefficient in the *Z* direction, α_{z_OOF}, is computed from the relative displacement change of the top and bottom of subsection. A temperature differential of 100 °C was used.

The coefficient of thermal expansion tensor was computed from the EBSD texture measurements in the Voigt approximation (Bunge 1982) in EBSD reference frame using the MTEX software.

Coefficients of thermal expansion from the experimental measurements were calculated from the dilations in the *X, Y,* and *Z* directions after the first heating from 20 to 90 °C for a temperature differential of 70 °C. The coefficient of thermal expansion was reconstructed from the thermal expansion values measured in six directions. The reconstructed tensor was rotated to EBSD reference frame in order to compare the results with coefficients from Voigt average calculations and OOF simulations.

Table 4 shows the modeled coefficients of thermal expansion α_{OOF}; the experimental values α_{expt} in the sample reference frame and in the EBSD reference frame; and coefficients of thermal expansion α_{Voigt} modeled from the texture measurements by applying the Voigt model for the investigated marbles.

The coefficients from the finite element simulations and those modeled from texture measurements show good directional correlation. Coefficients of thermal expansion obtained in thermal dilatation measurements are larger. Siegesmund et al. (2000) also observed larger experimental coefficients of thermal expansion and attributed the difference to be due primarily to the presence of microcracks, since they contribute an additional expansion. Since the computation simulations here do not allow the occurrence of microcracks, we expect the computational results to be smaller.

The MTEX software was also used to plot a pole figure projection of the thermal expansion tensor in any pole figure direction *X*, namely, $\alpha(X) = \langle \alpha_{ij} \rangle \cdot X_i \cdot X_j$.

Such thermal expansion pole figure plots were generated for both the experimental thermal expansion coefficients and the thermal expansion tensor computed from the EBSD texture measurements. The directional dependence of coefficients is evident in the Fig. 13, which shows the thermal expansion projection for the Sölk marble. Pole figures are shown for the thermal expansion tensor calculated from the EBSD measurements and for the experimentally measured tensor both in the sample reference frame and in the EBSD reference frame. The resemblance of Fig. 13a and c to the {001} pole figure in Fig. 5b is noted.

Summary and conclusions

The thermoelastic behavior of marble was modeled and experimentally measured. In the present study a combination of different techniques, such as finite-element simulations, EBSD measurements, and thermal expansion experiments, was used to elucidate the main factors, that leading to marble degradation. A significant observation is that the thermal behavior of marbles can be modeled in good agreement with experiments.

The effect of the different fabric parameters was investigated. The marble composition, grain size, grain boundary geometry. and texture significantly influence the thermal behavior of marble (Siegesmund et al. 2000; Zeisig et al. 2002; Weiss et al. 2002, 2003, 2004, Siegesmund et al. 2008; Shushakova et al. 2012). The present study revealed that fabric parameters and some of their combinations trigger a propensity for the thermal deterioration of marble.

Thermoelastic response maps showing the spatial dependence of the maximum principal stress, confirm that the Thassos dolomitic marble with strong texture (Fig. 12c) has a minimal tendency for microcracking. Indeed, finite-element modeling of Weiss et al. (2002) and Shushakova et al. (2012) and the systematic experimental study of Zeisig et al. (2002) indicated that dolomitic marbles are more resistance to thermal degradation due to the smaller crystalline thermal expansion anisotropy. Furthermore, with increasing LPO, microcracking is less prominent and occurs at a larger temperature differential (Shushakova et al. 2012). This observation is in good agreement with the results of the thermal expansion measurements. It was seen that marbles with strong texture exhibit minimal residual strain after the thermal treatment.

The grain size and grain boundary character do not play such important role in thermal degradation processes. The presence or absence of a residual strain after thermal treatment was independent of whether the marbles had a fine-grained size or a coarse-grained size. Furthermore, marbles with polygonal structure and interlobate grain boundaries do not show significant differences in their thermal expansion behavior.

It was observed that the texture controls the magnitude and directional dependence of the coefficient of thermal expansion, since coefficients that are modeled from texture are in a good agreement with experimental coefficients (see Table 4). Differences between the experimental values and the modeled ones are explained as the occurrence of microcracks during thermal treatment, which are not allowed in the modeling.

The influence of fabric parameters on residual strain upon thermal treatment, and hence on marble degradation, has been demonstrated. A major conclusion from both the modeling and the experimental findings is that the dolomitic marbles with strong texture are more resistant to marble thermal degradation.

Acknowledgments The authors gratefully acknowledge Grelk and Jan Anders Brundin for Fig. 1. Financial support for E. R. Fuller, Jr. at Universität Göttingen was provided by the Deutsche Forschungsgemeinschaft grant: SI 438/39–1, and is gratefully acknowledged. Victoria Shushakova gratefully acknowledges a long-term DAAD fellowship grant.

References

Bass JD (1995) Elasticity of minerals, glasses, and melts. In: Ahrens TJ (ed) Handbook of physical constants. American Geophysical Union, Washington, pp 45–63

Battaglia S, Franzini M, Mango F (1993) High sensitivity apparatus for measuring linear thermal expansion: preliminary results on the response of marbles. Il Nuovo Cimento 16:453–461

Bunge HJ (1982) Texture analysis in material sciences. Butterworth, London

Bunge HJ (1985) Representation of preferred orientations. In: Preferred orientation in deformed metals and rocks: an introduction to modern texture analysis. Academic Press, New York, pp 73–108

Carter WC, Langer SA, Fuller ER (1998) The OOF manual: version 1.0. National Institute of Standards and Technology (NIST), NISTIR No.6256

Chawla N, Patel BV, Koopman M, Chawla KK, Saha R, Patterson BR, Fuller ER, Langer SA (2003) Microstructure-based simulation of thermomechanical behavior of composite materials by object-oriented finite element analysis. Mater Charact 49:395–407

Grüneisen E (1926) Zustand des festen Körpers. In: Geiger H, Scheel K (eds) Handbuch der Physik, Bd. 10: Thermische Eigenschaften der Stoffe. Springer, Berlin

Halfpenny A (2010) Some important practical issues for the collection and manipulation of electron backscatter diffraction (EBSD) data from geological samples. In: Forster, MA, John D. Fitz Gerald (eds) The Science of Microstructure—Part I, J Virtual Explorer, Electronic edn, ISSN 1441-8142, vol 35, p 3, doi:10.3809/jvirtex.2011.00272

Hielscher R, Schaeben H (2008) A novel pole figure inversion method: specification of the MTEX algorithm. J Appl Crystallogr 41:1024–1037. doi:10.1107/S0021889808030112

Kessler DW (1919) Physical and chemical tests on the commercial marbles of the United States. Technologic Papers Bureau of Standards, No. 123, Government Printing Office, Washington

Kleber W (1959) Einfiihrung in die Kristallographie. VEB Verlag Technik, Berlin

Koch A, Siegesmund S (2004) The combined effect of moisture and temperature on the anomalous behaviour of marbles. Environ Geol 46:350–363

Langer SA, Fuller ER, Carter WC (2001) OOF: an image-based finite element analysis of material microstructures. Comput Sci Eng 3:15–23. (OOF is freely available at http://www.ctcms.nist.gov/oof/)

Leiss B, Molli G (2003) High-temperature texture in naturally deformed Carrara marble from Alpi Apuane, Italy. J Struct Geol 25:649–658

Leiss B, Ullemeyer K (1999) Texture characterisation of carbonate rocks and some implication for the modeling of physical anisotropies, derived from idealized texture types. Z Deut Geol Ges 150:259–274

Luque A, Ruiz-Agudo E, Cultrone G, Sebastián E, Siegesmund S (2011) Direct observation of microcrack development in marble caused by thermal weathering. Environ Earth Sci 62(7):1375–1386

Mainprice D, Hielscher R, Schaeben H (2011) Calculating anisotropic physical properties from texture data using the MTEX open source package. In: Prior DJ, Rutter EH, Tatham DJ (eds) Deformation mechanisms, rheology and tectonics: microstructures, mechanics and anisotropy. Geological Society, London, Special Publications 360, pp 175–192

Rabinowitzt M, Carr J (2012) The New York public library statuary-marble deterioration and conservation. In: 12th International congress on deterioration and conservation of stone, New York (in print)

Reeder R, Markgraf SA (1986) High temperature crystal chemistry of dolomite. Am Mineral 71:795–804

Ritter H (1992) Die Marmorplatten sind falsch dimensioniert. Stein H. 1/1992:18–19

Ruedrich J (2003) Gefügekontrollierte Verwitterung natürlicher und konservierter Marmore. Dissertation, Universität Göttingen, 158 S

Ruedrich J, Weiss T, Siegesmund S (2002) Thermal behaviour of consolidated marbles. In: Siegesmund S, Weiss T, Vollbrecht A (eds) Natural stone, weathering phenomena, conservation strategies and case studies. Geological Society Special Publication No. 205, The Geological Society of London, London, pp 255–271

Saylor DM, Fuller ER, Weiss T (2007) Thermal-elastic response of marble polycrystals: influence of grain orientation configuration. Int J Mat Res (formerly Z. Metallkd.) 98(12):1256–1263

Shushakova V, Fuller ER, Siegesmund S (2011) Influence of shape fabric and crystal texture on marble degradation phenomena: simulations. Environ Earth Sci 63:1587–1601

Shushakova V, Fuller ER, Siegesmund S (2012) Microcracking in calcite and dolomite marble: microstructural influences and effects on properties. Environ Earth Sci. doi:10.1007/s12665-012-1995-2

Siegesmund S, Weiss T, Vollbrecht A, Ullemeyer K (1999) Marble as a natural building show: rock fabrics, physical and mechanical properties. Z Dtsch Geol Ges 150:237–257

Siegesmund S, Ullemeyer K, Weiss T, Tschegg EK (2000) Physical weathering of marbles caused by anisotropic thermal expansion. Int J Earth Sci 89:170–182

Siegesmund S, Ruedrich J, Koch A (2008) Marble bowing: comparative studies of different public building facades. In: Siegesmund S, Snethlage R, Ruedrich J (eds) Monumental future: climate change, air pollution, stone decay and conservation. Environ Geol, vol 56, pp 473–494

Trewitt TJ, Tuchmann J (1988) Amoco may replace marble on Chicago headquarters. ENR March: 11–12

Tschegg E, Widhalm C, Eppensteiner W (1999) Ursachen mangelnder Formbestaetigkeit von Marmorplatten. Zeitschrift der Deutschen Geologischen Gesellschaft 150(2):283–297

Wanner T, Fuller ER, Saylor DM (2010) Homology metrics for microstructure response fields in polycrystals. Acta Mater 58:102–110

Weiss T, Siegesmund S, Fuller ER (2002) Thermal stresses and microcracking in calcite and dolomite marbles via finite element modelling. In: Siegesmund S, Weiss T, Vollbrecht A (eds) Natural stone, weathering phenomena, conservation strategies and case studies. Geological Society Special Publication No. 205, The Geological Society of London, London, pp 89–102

Weiss T, Siegesmund S, Fuller ER (2003) Thermal degradation of marble: indications from finite-element modelling. Build Environ 38(9–10):1251–1260

Weiss T, Saylor DM, Fuller ER, Siegesmund S (2004) Prediction of the degradation behaviour of calcareous rocks via finite-element modelling. In: 10th International congress on deterioration and conservation of stone, Stockholm, pp 163–170

Widhalm C, Tschegg E, Eppensteiner (1996) Anisotropic thermal expansion causes deformation of marble cladding. J Perform Constr Facil 10:5–10

Zeisig A, Siegesmund S, Weiss T (2002) Thermal expansion and its control on the durability of marbles. In: Siegesmund S, Weiss T, Vollbrecht A (eds) Natural stone, weathering phenomena, conservation strategies and case studies. Geological Society Special Publication No. 205, The Geological Society of London, London, pp 65–80